ACS APPLIED ELECTRONIC MATERIALS

pubs.acs.org/acsaelm

Article

Influence of the Interface on the Electric Control of the Magnetization Direction in Fe/PMN-PT Magnetoelectric Heterostructures

Michelle Rodrigues,* Sergey Basov, Ivan Madarevic, Thomas Saerbeck, Matteo Ferroni, Patrick Breckner, Daniel Isaia, Lovro Fulanović, Atefeh Jafari, Ilya Sergueev, Olaf Leupold, Margriet J. Van Bael, André Vantomme, and Kristiaan Temst

Cite This: *ACS Appl. Electron. Mater.* 2024, 6, 2289−2300

Read Online

ACCESS | Metrics & More | Article Recommendations

ABSTRACT: The magnetization direction of a ferromagnetic (FM) film deposited onto a ferroelectric (FE) substrate undergoes significant changes when it is subjected to applied electric fields. These are mainly due to the strain-mediated magnetoelectric effects associated with the FE switching behavior of the substrates. Here, we report on the magnetoelectric response of the magnetization direction at two different depths within the FM film in an artificial multiferroic heterostructure consisting of a 5 nm FM Fe film deposited onto a 0.7Pb($Mg_{1/3}Nb_{2/3}$)O_3-0.3$PbTiO_3$ (PMN-PT) FE single-crystal substrate. The overall magnetic anisotropy of the Fe (5 nm)/PMN-PT system was studied by using magneto-optic Kerr effect (MOKE) magnetometry. On the other hand, the isotope-specific nuclear forward scattering (NFS) of synchrotron radiation was used to study the magnetization direction at two specific depths within the Fe film. Our results reveal that magnetic anisotropy is significantly influenced by the Fe/PMN-PT interface. Additionally, the magnetoelectric response of the easy magnetization direction when the layer is simultaneously subjected to electric and magnetic fields is different at (1st nm of Fe) as compared to away (3rd nm of Fe) from the Fe/PMN-PT interface. At the interface, the magnetization direction is influenced by the electric field-induced strain and charge effects originating in PMN-PT. Away from the interface, a weaker magnetoelectric response of the magnetization direction consistent with previous reports is observed. These results provide insight in understanding the magnetoelectric coupling behavior of such FM/PMN-PT heterostructures, which is crucial to recognize their potential in developing (multi)functional devices based on such systems.

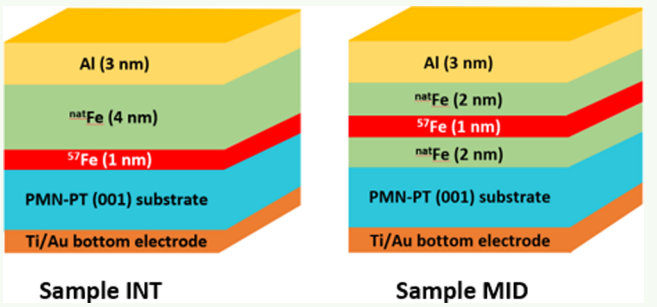

KEYWORDS: *magnetoelectric, multiferroics, heterostructures, interfaces, nuclear resonant scattering, magnetization direction*

INTRODUCTION

Electric-field control of magnetism is essential for achieving high-density, fast-switching, nonvolatile, and low power-consuming magnetic memory and spintronic devices.[1−4] Therefore, research is conducted on materials that are capable of controlling their coupled magnetic and electric properties, i.e., magnetoelectric (ME) materials.[3−9] Some compounds (single-phase multiferroics) show ME coupling; however, this coupling is most often rather weak and occurs at low ordering temperatures, making them less suitable for immediate practical applications.[10,11] Nevertheless, these single-phase multiferroics are still heavily researched due to their high technological relevance for a novel, low power-consuming magnetoelectric random access memory (MeRAM)[12,13] and, more recently, a novel magnetoelectric spin−orbit (MESO)[9,14] logic device.[4,15] To overcome the low ME coupling of single-phase multiferroics at room temperature, artificial multiferroic heterostructures that couple ferroelectric and magnetic materials via an interface are widely studied.[3,16−18] Such magnetoelectric heterostructures are better suited for immediate practical applications, e.g., as sensors, radio and high-frequency devices, energy harvesters, etc.[3,19−21]

Specifically, in ferromagnetic (FM)/ferroelectric (FE) artificial multiferroic heterostructures, the FM/FE interface is a crucial component as it determines the different underlying coupling mechanisms that govern the ME coupling in these systems.[3] Moreover, at an FM/FE interface, the strain and

Received: December 20, 2023
Revised: March 22, 2024
Accepted: March 25, 2024
Published: April 8, 2024

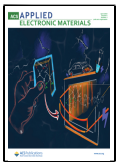

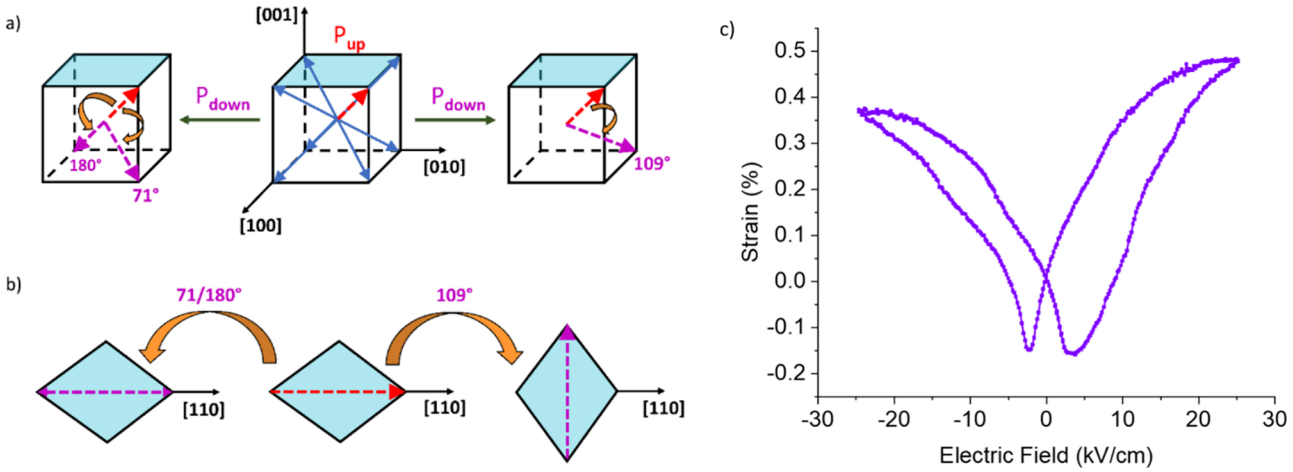

Figure 1. Schematics of 71°/180° and 109° polarization switching in a pseudocubic unit cell of (001)-oriented PMN-PT: (a) 3D representation and (b) in-plane projections of the corresponding polarization switching processes in the shaded (001)-surface plane. (c) Out-of-plane strain−electric field (S−E) curve for the (001)-oriented PMN-PT substrate recorded along the PMN-PT [001] direction.

charge ME coupling mechanisms can coexist, which complicates the understanding of the ME coupling in these systems.[22,23] For example, the charge- or carrier-mediated ME mechanism involves electric field-induced modification of the interfacial charge density, which is screened by the accumulation/depletion of electrons in the FM layer.[24] Additionally, in 3d metals, the charge effect can vary the number of 3d electrons, which can in turn significantly alter the magnetic anisotropy.[3] However, although capable of inducing a significant magnetic reconstruction, the charge-mediated effect is confined to the close proximity of the FM/FE interface due to the relatively short screening length of FM metals. On the other hand, the strain-mediated mechanism involves the transfer of the electric field-induced strain from the FE into the FM via the interface, which in turn modifies magnetic anisotropy via inverse piezoelectricity and magnetostriction.

To fabricate artificial ME heterostructures, relaxor ferroelectrics like $[Pb(Mg_{1/3}Nb_{2/3})O_3]_{1-x}$-$[PbTiO_3]_x$ are very suitable as FE substrates due to their large dielectric and piezoelectric coefficients.[25,26] Specifically, Pb-$(Mg_{1/3}Nb_{2/3})_{0.7}Ti_{0.3}O_3$ (hereafter, PMN-PT) exhibits superior piezoelectric properties, making it the FE substrate of choice for many ME investigations.[27−39] Polarization in unpoled rhombohedral PMN-PT lies along the ⟨111⟩ pseudocubic body diagonals. An electrically driven out-of-plane polarization change in PMN-PT can result in 71°, 180°, or 109° rotation of the polarization vector, corresponding to the angles between the different ⟨111⟩ pseudocubic directions. For (001)-oriented PMN-PT, when an electric field is applied out of plane along the [001]-direction, 71° or 180° polarization switching leads to an in-plane butterfly-like strain response.[25] Initially, the FE undergoes a tensile strain due to polarization tilting out of plane and reaches a maximum at the electric coercive field, where polarization switches after which the strain decreases and becomes compressive until the maximum applied electric field value is attained. Ramping down the electric field reverts the strain to zero, which implies that the in-plane butterfly strain associated with 71° or 180° polarization switching is volatile in nature. Since the volume change of the FE has to be maintained under the application of the electric fields, when the strain response is recorded along the out-of-plane direction, a complementary butterfly strain, which is inverted with respect to the in-plane butterfly strain, is observed. Moreover, the volatile strain in turn has a volatile effect on the in-plane magnetic anisotropy of the FM film in such FM/PMN-PT heterostructures since the changes in anisotropy due to the strain transfer revert to zero as the strain reverts to zero upon removal of the applied electric field.[25] In contrast, if polarization switches by 109°, then the corresponding in-plane effect is seen as a 90° rotation of the long diagonal, giving rise to looplike behavior associated with the ferroelastic strain.[28,34] The looplike strain associated with 109° polarization switching is nonvolatile (two different strain states at a zero electric field), which leads to the desirable nonvolatile ME effect whereby the easy axis of magnetization of the FM rotates by 90° in-plane.[28,32−37] A schematic representation of polarization switching in (001)-oriented PMN-PT is depicted in Figure 1 a,b.[3,28] It was recently reported[40] for a Ni(10 nm)/(011)-$PMN_{0.68}$-$PT_{0.32}$ system that although the in-plane global magnetic easy axis rotates by the expected 90° via the strain-induced ME effect, the magnetization direction on the surface of the Ni (10 nm) film rotated between 62° and 84°. This sub-90° rotation of surface magnetization was attributed to the competing in-plane shear strain (∼0.14%) associated with ferroelectric domain switching.[40] Local Ni surface magnetization was studied using X-ray magnetic circular dichroism−photoemission electron spectroscopy (XMCD-PEEM) imaging, which allows vector mapping of in-plane magnetization. Using the same technique, it was reported[35] for an Fe (4 nm)/(001)-$PMN_{0.6}$-$PT_{0.4}$ system that the magnetization direction on the surface of an Fe film also undergoes non-90° rotations, which were mainly linked to the electrically induced morphological changes (crack formation[41]) in the substrate. Additionally, the electric field-induced rotation of the magnetization direction was not uniform over the Fe film surface, and it is expected to orient itself perpendicular to the propagation direction of the electric field-induced cracks.[35] These reports[35,40] discuss and suggest that the average/global magnetoelectric response of the magnetic easy axis in FM/PMN-PT heterostructures is different from that observed microscopically on the surface of the FM film. Additionally, these reports hint that the magnetoelectric response at the FM/FE interface compared to a few nanometers away from it

https://doi.org/10.1021/acsaelm.3c01800
ACS Appl. Electron. Mater. 2024, 6, 2289−2300

within the FM film in such heterostructures might be different, which has not yet been reported.

In this work, we investigate the behavior of the magnetization direction at two different depths within the FM of an FM/FE magnetoelectric heterostructure when subjected to simultaneous application of *in situ* electric and magnetic fields. We show that the interfacial region contributes significantly to the total magnetic anisotropy of the FM/FE heterostructure. We report on the room-temperature variation of the magnetization direction resulting from the ME coupling effects in an artificial multiferroic heterostructure composed of a 5 nm Fe film deposited on a single-crystal (001)-oriented PMN-PT substrate. We use magneto-optic Kerr effect (MOKE) magnetometry to measure the initial (postgrowth) in-plane magnetic anisotropy of the 5 nm Fe film. The electric-field effect on the magnetization direction at specific depths within the Fe film, i.e., at the first and third nm of Fe (referred to as at and away from the Fe/PMN-PT interface, respectively, in the remainder of this paper), was studied using the well-established,[42−48] isotope-sensitive nuclear resonant scattering (NRS) of synchrotron radiation. Alongside previously reported[35,40] differences between the magnetoelectric responses of the global and surface magnetization directions, our results demonstrate depth-specific behavior in such FM/FE systems, which we investigate by inserting an isotopically pure ^{57}Fe probe layer at two different depths within the Fe film (once at and once farther away from the FM/FE interface).

EXPERIMENTAL SECTION

Single-crystal relaxor FE (001)-oriented $PMN_{(1-x)}$-PT_x 10 × 10 × 0.5 mm^3 in size with x = 0.3 (SurfaceNet GmbH, Rheine, Germany) was selected as the substrate due to its strong piezoelectric properties (longitudinal piezoelectric coefficient, d_{33} = 2200−2500 pC/N).[25−27] At room temperature, in this composition, PMN-PT is located at the morphotropic phase boundary and possesses a rhombohedral crystal structure with lattice parameters of a = 4.017 Å and θ = 89.97°.[26] Molecular beam epitaxy (MBE) was used to grow the FM Fe film as a combination of an isotopically pure ^{57}Fe probe layer (∼1 nm) and natural Fe (^{nat}Fe) layers (natural referring to the natural abundance of all Fe isotopes), with a total Fe layer thickness of 5 nm. The ^{57}Fe probe layer combined with the isotope-specific nuclear resonant scattering technique is crucial to probe the magnetic response locally at specific depths within the Fe film—in particular at the buried Fe/PMN-PT interface. To study the Fe/PMN-PT interface, Sample INT was grown with Al (3 nm)/^{nat}Fe (4 nm)/^{57}Fe (1 nm)/PMN-PT, i.e., with the ^{57}Fe probe layer at the interface (INT). To study the effects further away from the interface, Sample MID was grown with Al (3 nm)/^{nat}Fe (2 nm)/^{57}Fe (1 nm)/^{nat}Fe (2 nm)/PMN-PT where the ^{57}Fe probe layer is deposited 2 nm away from the Fe/PMN-PT interface, hence, in the middle (MID) of the Fe layer. The growth was conducted at 50 °C with a base pressure < 10^{-9} mbar and was monitored *in situ* using reflection high-energy electron diffraction (RHEED). The samples were capped with 3 nm Al to prevent oxidation of the Fe layers while also serving as the top electrode for the application of electric fields. A Ti/Au bilayer was deposited at the back of the PMN-PT substrate, which served as the bottom electrode. A schematic of the sample structure is depicted in Figure 2.

The electric field-induced axial strain (S_{33}) response (S−E curve) of the bare PMN-PT substrate was measured at room temperature by using linear differential variable transducers (LVDTs). Ti/Au electrodes were deposited on the opposite [001] faces of the PMN-PT substrate, which was mounted in a silicone oil bath. The LVDTs measure displacement due to applied electric fields along the loading direction, i.e., in this case, the [001]−PMN-PT direction. The displacement was measured at a frequency of 0.1 Hz, generated with a data acquisition card (National Instruments) and high-voltage

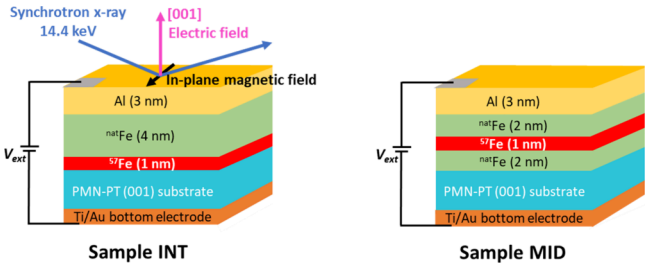

Figure 2. Schematic of the samples analyzed using NFS, which is only sensitive to the ^{57}Fe probe nuclei and is blind to other isotopes of Fe present in the ^{nat}Fe layers. In sample INT (Sample MID), the ^{57}Fe probe layer is present at (away from) the Fe/PMN-PT interface (thicknesses are not to scale). Sample INT also shows the sample environment in the NFS setup where the in-plane magnetic field is applied perpendicular to the direction of propagation of the synchrotron X-ray beam. The electric field is applied out of plane, along the [001]-direction with respect to the PMN-PT substrate.

amplifier (Trek 20/20). The crystallinity of Sample INT and Sample MID was characterized using transmission electron microscopy (TEM). TEM cross-sectional lamellae (∼150 nm thick) of the samples were prepared by a focused beam of Ga ions. Pt was deposited on the samples for protection of microstructural features during lamella fabrication. In-plane magnetic hysteresis loops averaging over the 5 nm Fe thickness at E = 0 kV/cm were recorded on Sample INT and Sample MID using a magneto-optic Kerr effect (MOKE) magnetometer in the longitudinal configuration. The loops were measured at 10° intervals of in-plane magnetic field orientation with respect to the [100]−PMN-PT direction and were further normalized to saturation magnetization. From the angular dependence of the ratio of remnant magnetization (M_r) and saturation field (M_s), derived from the hysteresis loops—also referred to as the squareness ratio (M_r/M_s)—global in-plane magnetic anisotropy for the Fe/PMN-PT system was deduced in the post-growth or electrically pristine state, i.e., at E = 0 kV/cm.

The local variation of the in-plane magnetization direction at and away from the Fe/PMN-PT interface was studied using nuclear resonant scattering (NRS) of synchrotron radiation at the beamline P01 at the Petra III synchrotron (DESY, Hamburg[49]) where we benefit from the large photon flux of the brilliant synchrotron X-ray beam and the possibility to simultaneously apply *in situ* electric and magnetic fields. NRS, a well-established[42−48] and unique tool for studying magnetism in (ultra)thin films, is analogous to Mössbauer spectroscopy—a nuclear spectroscopy technique where the spectroscopic pattern is highly sensitive to the magnetic and chemical states of the probe nuclei under study[50,51]—and is sensitive to Mössbauer nuclei only (in this case, ^{57}Fe nuclei, but blind to the other Fe isotopes).[43,44,49] In this work, the NRS experiments were conducted in grazing incidence geometry with an incidence angle of 3.6 mrad and a beam spot size of 90 μm × 200 μm focused on the sample surface. The grazing incidence mode allows for increased surface sensitivity, which makes the NRS technique especially useful for studying (ultra-)thin film systems that suffer from an inherent low sample volume problem. The synchrotron X-ray beam was tuned to 14.4 keV to trigger the response from the ^{57}Fe nuclei present in the probe layer of the samples. This energy corresponds to the magnetic dipole transition of the ^{57}Fe nuclei from the ground state (I_g = 1/2) to the excited state (I_e = 3/2), which has a natural lifetime of 141 ns. The synchrotron source produces short and intense pulses of photons that irradiate the sample periodically. The NRS measurements are time-resolved, and hence, temporal spacing between the consecutive synchrotron radiation pulses is a crucial experimental requirement. In this work, the synchrotron was operated in 40-bunch mode with 192 ns bunch separation.[49] Si avalanche photodiode detectors that have an ∼1 ns time resolution were used to register the scattered signal. It consists of information about both the electronic and nuclear reflectivity of the ^{57}Fe probe layer that occurs in different time

https://doi.org/10.1021/acsaelm.3c01800
ACS Appl. Electron. Mater. 2024, 6, 2289−2300

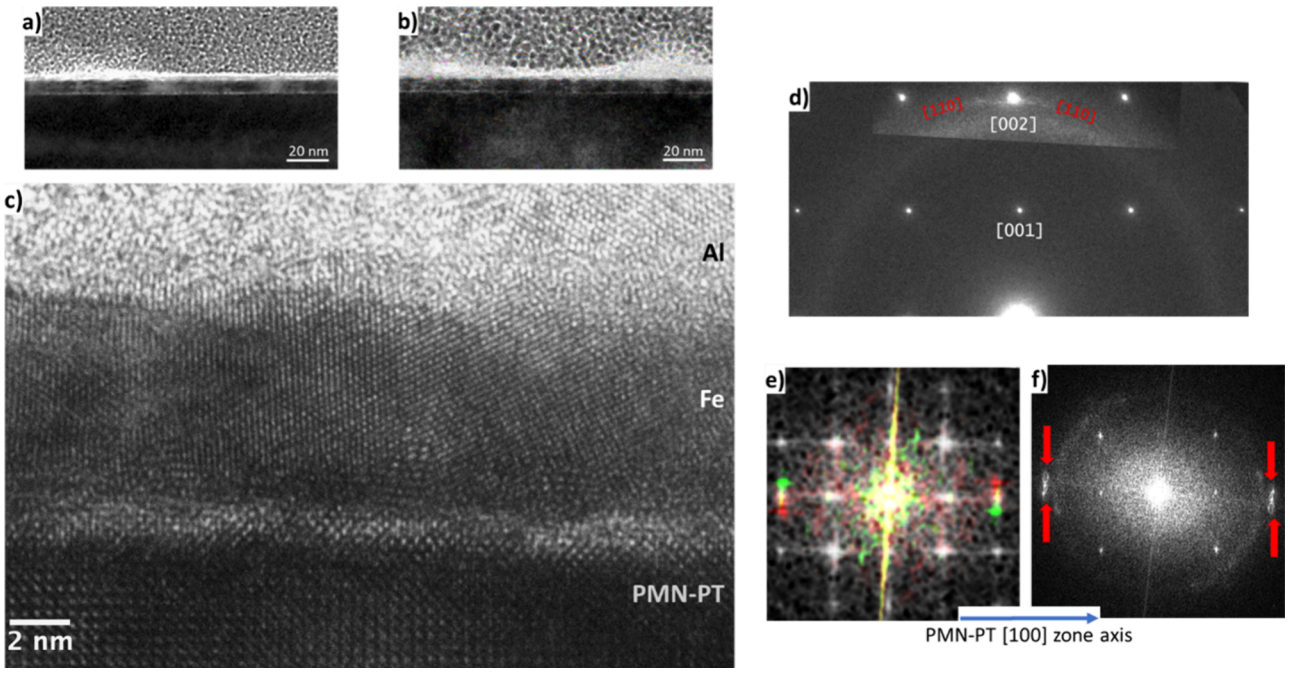

Figure 3. Transmission electron microscopy (TEM) of Sample INT and Sample MID. Bright-field TEM images of (a) Sample INT and (b) Sample MID. (c) High-resolution TEM image of Sample INT. (d) Montage of two selected-area electron diffraction (SAED) patterns, acquired at different exposures. The preferential orientation of the nanosized Fe grains is revealed by a faint arc of diffraction intensity from $[110]_{Fe}$ planes of the Fe layer (red) that are symmetrically distributed around the $[002]_{PMN\text{-}PT}$ diffraction spot. (e) Fourier transform of the HR-TEM image (c) of Sample INT showing the preferential orientation of the Fe grains. The red and green spots come from the FFT of two regions of the Fe layer and correspond to the $[110]_{Fe}$ spatial frequencies that are nearly aligned with that of the $[200]_{PMN\text{-}PT}$ substrate. (f) Fourier transform from the HR-TEM image of Sample MID showing a similar preferential orientation of the Fe grains: the red arrows mark the diffraction intensity arising from the $[110]_{Fe}$ grains, which are symmetrically distributed around the $[200]_{PMN\text{-}PT}$ diffraction spots.

ranges. The photons detected in the first 20 ns after the synchrotron X-ray pulse correspond to prompt electronic scattering and are therefore discarded, whereas the counts that follow, i.e., after 20 ns, correspond to nuclear resonant scattering (NRS time spectra) from the ^{57}Fe probe nuclei. Nuclear scattering, i.e., the NRS response, is delayed in time due to the finite lifetime of the excited state, which is 141 ns in the case of ^{57}Fe. The recorded NRS spectra therefore represent the decaying intensity of the excited ^{57}Fe nuclei as a function of time.[44] It consists of oscillations that are referred to as a quantum beating pattern associated with the strength of the hyperfine splitting of ^{57}Fe nuclear states, which depends on the orientation of the magnetic moment with respect to the direction and polarization of the synchrotron X-ray beam.[42−44] Since these hyperfine interactions are determined by the nearest-neighbor interactions, NRS allows probing the magnetization locally. To deduce the hyperfine parameters such as the magnetic hyperfine field (B_{hf}) and its direction, the isomer shift, and quadrupole splitting from the ^{57}Fe probe layer at and away from the Fe/PMN-PT interface, the NRS spectra were fitted using the CONUSS software package,[52] which is a forward simulator based on the theoretical description given in ref 53. It should be stressed that since the NRS spectra originate from the interference of transitions with slightly different energy, a direct visual interpretation of (minute variations of) the spectra is basically impossible, making it absolutely necessary to analyze the data in conjunction with simulations and fittings. The ^{57}Fe probe layer strategy combined with the NRS of synchrotron radiation experiments therefore allows one to locally probe nanoscale magnetism and magnetoelectric phenomena at different depths within magnetic thin films and artificial multiferroic heterostructures with (sub)nm sensitivity, which cannot be achieved using volume- and surface-sensitive magnetometry measurements.[43,45−48]

The NRS measurement configuration will henceforth be referred to as NFS (nuclear forward scattering) due to the geometry of the incident and reflected synchrotron X-ray beam, as depicted in Figure 2. In the NFS experiments, the electric field was applied out of plane, along the [001]-direction with respect to the PMN-PT substrate. The magnetic field (100 mT) was applied in-plane along the [010]-direction of the PMN-PT substrate (magnetic hard axis), and it is orthogonal to the direction of the synchrotron X-ray beam (Figure 2). Starting from an electrically pristine state, the samples are first subjected to negative electric poling to a maximum of −16 kV/cm, which is well beyond the electric coercive field of the PMN-PT substrate ($E_c \approx \pm 2$ kV/cm[34]). Subsequently, the electric field is decreased to the remanent polarization state (0^-) and then the samples are positively poled to a maximum of +16 kV/cm, followed by decreasing the electric field to the final remanent polarization state (0^{-+}). At each applied electric field value and at both remanent polarization states (0^- and 0^{-+}), two NFS spectra were recorded: one in the magnetic field (100 mT) and another in magnetic remanence (∼0 mT) after removing the applied magnetic field. No spectra were recorded during the ramping down of the electric fields.

RESULTS AND DISCUSSION

Structural Characterization of Ultrathin Fe (5 nm) Films. The TEM results of Sample INT and Sample MID are listed in Figure 3. The bright-field (BF) TEM images of Sample INT and Sample MID depict a continuous and uniform Fe film with a clear film−substrate interface. As the TEM electron beam was preliminary aligned along the PMN-PT [010] zone axis, the contrast in this image allows for visual identification of grains within the Fe film that are close to the condition for Bragg diffraction. For Sample INT and Sample MID, the Fe film in the BF-TEM images (Figure 3 a,b) depicts both bright and dark regions, implying that it is mainly polycrystalline with nanosized Fe grains.

Figure 3 c depicts the high-resolution TEM (HR-TEM) of Sample INT. It highlights that the Al capping layer is amorphous, while the Fe layers show contrast fringes, arranged

https://doi.org/10.1021/acsaelm.3c01800
ACS Appl. Electron. Mater. 2024, 6, 2289−2300

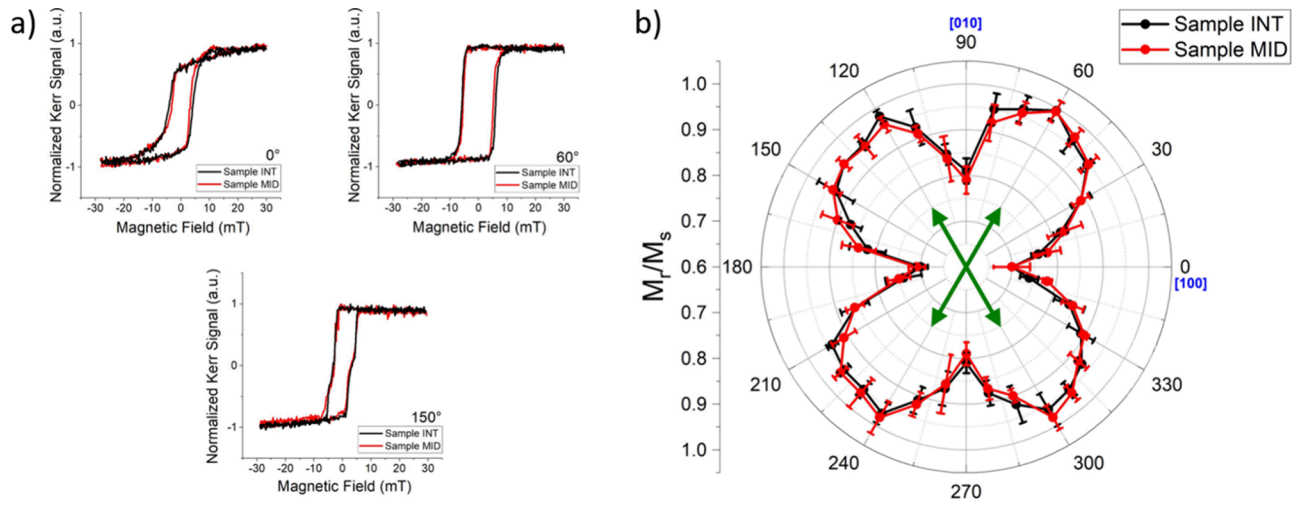

Figure 4. Magnetic characterization of the 5 nm Fe film in Sample INT and Sample MID by longitudinal MOKE at E = 0 kV/cm. (a) Hysteresis loops at different in-plane magnetic field orientations and (b) angular dependence of the squareness ratio (M_r/M_s) derived from the hysteresis loops depicting the in-plane easy axes (green arrows) of magnetic anisotropy.

in patterns of parallel lines that visualize the ordered arrangement of the Fe layer. The bottom of the HR-TEM image showing the lattice planes of the underlying PMN-PT substrate is a clear visualization of its single-crystalline structure. Generally, for an Fe film (lattice parameter a_{Fe} = 2.866 Å) deposited on PMN-PT ($a_{PMN\text{-}PT}$ = 4.017 Å), to reduce the lattice mismatch, it is energetically favorable for Fe to grow with its lattice azimuthally rotated in-plane by 45° with respect to the substrate since $\sqrt{2}\,a_{Fe}$ = 4.053 Å.[34,39] Therefore, the expected relationship between the Fe film and the (001)-oriented PMN-PT substrate is Fe [110]||PMN-PT [100]. To verify if such a preferred orientation exists in the polycrystalline Fe films studied in this work, the HR-TEM image of Sample INT (Figure 3 c) is further analyzed by electron diffraction. Figure 3 d depicts the selected area electron diffraction (SAED) pattern from the HR-TEM image of Sample INT (Figure 3 c). A superposition of two SAED patterns acquired at different exposures was derived to enhance the visibility of the diffraction intensity arising from the ultrathin Fe film. Indeed, a preferential orientation of the nanometric Fe grains exists and is revealed by a faint arc of diffraction intensity coming from $[110]_{Fe}$ planes, which are symmetrically distributed around the $[002]_{PMN\text{-}PT}$ diffraction spot.

A complementary approach to investigating the preferential orientation of the Fe grains at the nanometer scale is to generate the fast Fourier transformation (FFT) of the HR-TEM image. The color-enhanced image in Figure 3 e is a montage of three FFTs obtained from different areas of the cross section. The gray image shows the FFT of the substrate fringes. The red and green diffraction spots come from the FFT spectra of two regions of the Fe layer. They correspond to the $[110]_{Fe}$ spatial frequencies that are nearly aligned with that of the $[200]_{PMN\text{-}PT}$ substrate, giving rise to evidence of the expected[34,39] Fe [110]||PMN-PT [100] relationship. These results complement the SAED pattern in Figure 3 d and are further evidence of the preferential orientation of the Fe film with respect to the underlying PMN-PT substrate. Similarly, the Fe [110]||PMN-PT [100] orientation was also found in Sample MID, as reported by the SAED pattern in Figure 3 f.

Magnetic Anisotropy of Fe (5 nm)/PMN-PT at E = 0 kV/cm. The dominance of the Fe [110]||PMN-PT [100] crystallographic relationship should give rise to a system where the in-plane magnetic easy axes of Fe lie along 45° with respect to the PMN-PT crystallographic [100] and [010] directions in the post-growth, E = 0 kV/cm state.[34,39] To verify this and study the in-plane magnetic anisotropy of the Fe (5 nm)/PMN-PT system in this work, Sample INT and Sample MID were analyzed at E = 0 kV/cm using MOKE magnetometry. Since MOKE is not an isotope-specific technique, it cannot differentiate between the ^{nat}Fe and ^{57}Fe layers and is therefore only sensitive to the signal from the 5 nm film of Fe as a whole. This further implies that the magnetic characterization of Sample INT and Sample MID with the probe layer at and away from the Fe/PMN-PT interface is expected to be identical when analyzed using MOKE magnetometry.

Figure 4 a depicts examples of the magnetic hysteresis loops recorded using longitudinal MOKE magnetometry for Sample INT and Sample MID. As expected, the magnetic response of the two samples analyzed using the non-isotope-specific technique of MOKE is confirmed to be the same. The loops recorded with the applied magnetic field oriented along 0° (||[100]−PMN-PT edge) show an asymmetric hysteresis loop. This asymmetry is due to the intermixing of antisymmetric transverse contributions with the symmetric longitudinal magnetization component in the MOKE setup as a result of quadratic magneto-optical effects.[54,55] These effects are not related to the inherent magnetic response of the sample.[54,55] The polar plot of M_r/M_s depicting the in-plane magnetic anisotropy of Sample INT and Sample MID at E = 0 kV/cm is presented in Figure 4 b. It shows that the anisotropy of the Fe/PMN-PT system follows the expected 4-fold magnetocrystalline anisotropy for body-centered cubic Fe. This further implies that the Fe film shows a preferred orientation with the PMN-PT substrate bearing the dominant Fe [110]||PMN-PT [100] crystallographic relationship. Additionally, it is clear that the easy axes do not lie exactly along the in-plane PMN-PT ⟨110⟩ directions, i.e., they do not lie along the in-plane 45° directions as expected from previous Fe/PMN-PT reports.[34,39] Moreover, for a system with perfect 4-fold magnetic anisotropy, the four minima in the M_r/M_s polar plot should be equivalent. In contrast, we observe that the M_r/M_s values along the PMN-PT ⟨010⟩ directions are somewhat larger than

https://doi.org/10.1021/acsaelm.3c01800
ACS Appl. Electron. Mater. 2024, 6, 2289−2300

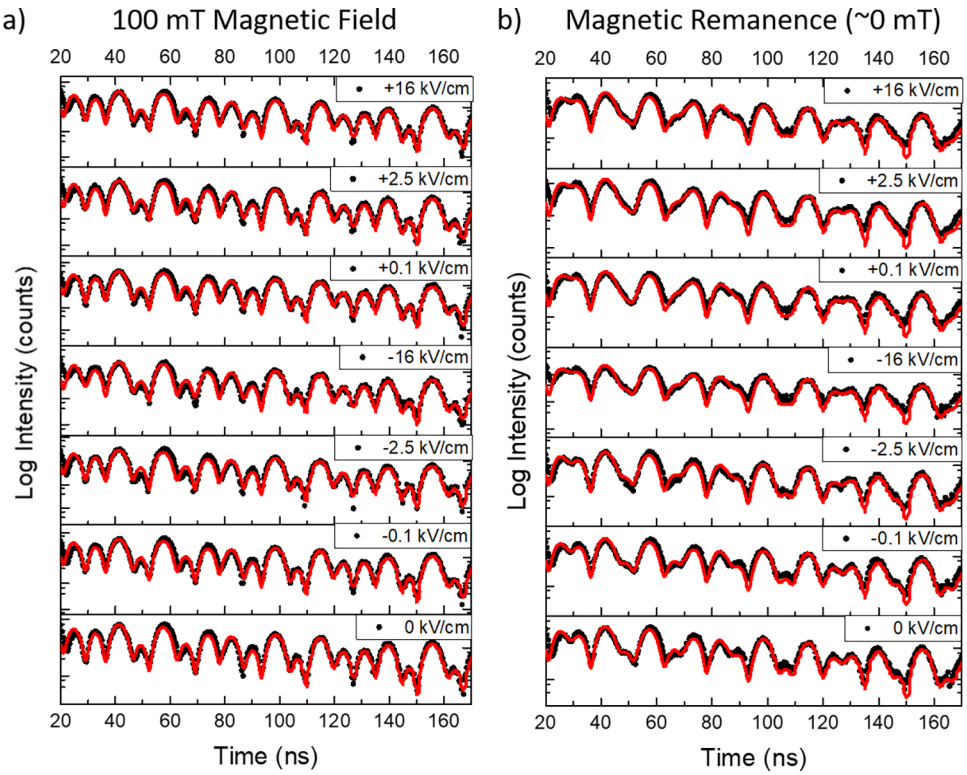

Figure 5. NFS time spectra of Sample INT (Al (3 nm)/^{nat}Fe (4 nm)/^{57}Fe (1 nm)/PMN-PT) with the ^{57}Fe probe layer at the interface: (a) under simultaneous application of electric and 100 mT magnetic fields and (b) in magnetic remanence after applying 100 mT. The solid lines (red) represent the fits to the data (black dots).

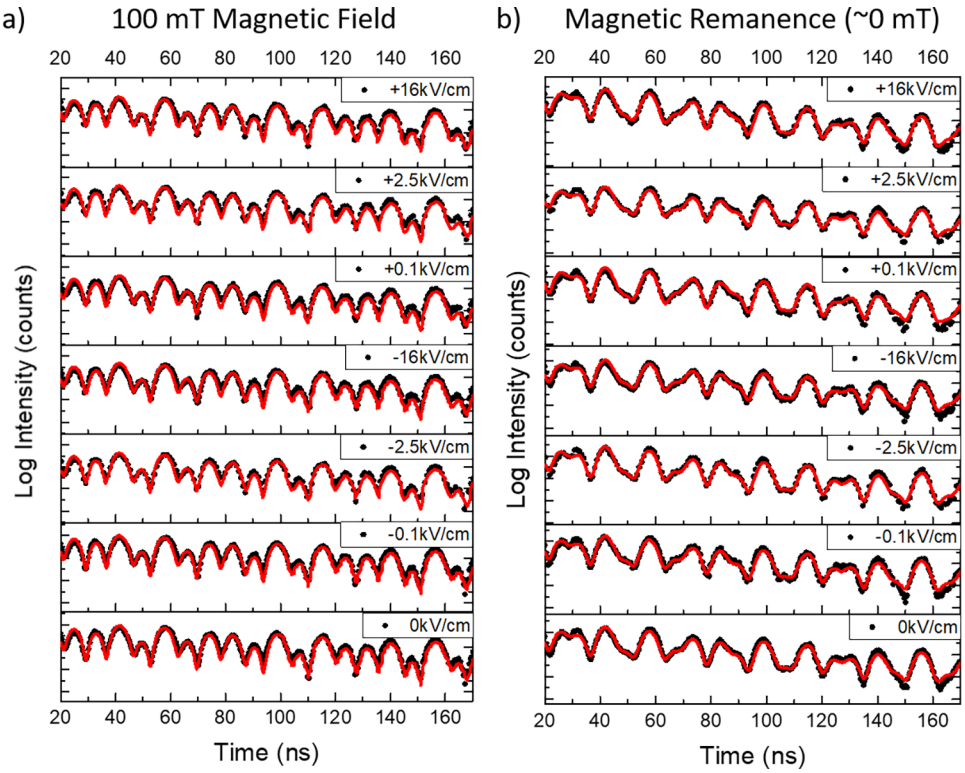

Figure 6. NFS time spectra of Sample MID (Al (3 nm)/^{nat}Fe (2 nm)/^{57}Fe (1 nm)/^{nat}Fe (2 nm)/PMN-PT) with the ^{57}Fe probe layer 2 nm away from the interface: (a) under simultaneous application of electric and 100 mT magnetic fields and (b) in magnetic remanence after applying 100 mT. The solid lines (red) represent the fits to the data (black dots).

those along the PMN-PT ⟨100⟩ direction (Figure 4 b). This elongation of the M_r/M_s polar plot is attributed to the presence of an additional uniaxial magnetic anisotropy component superimposed on the dominant 4-fold magnetocrystalline

https://doi.org/10.1021/acsaelm.3c01800
ACS Appl. Electron. Mater. 2024, 6, 2289−2300

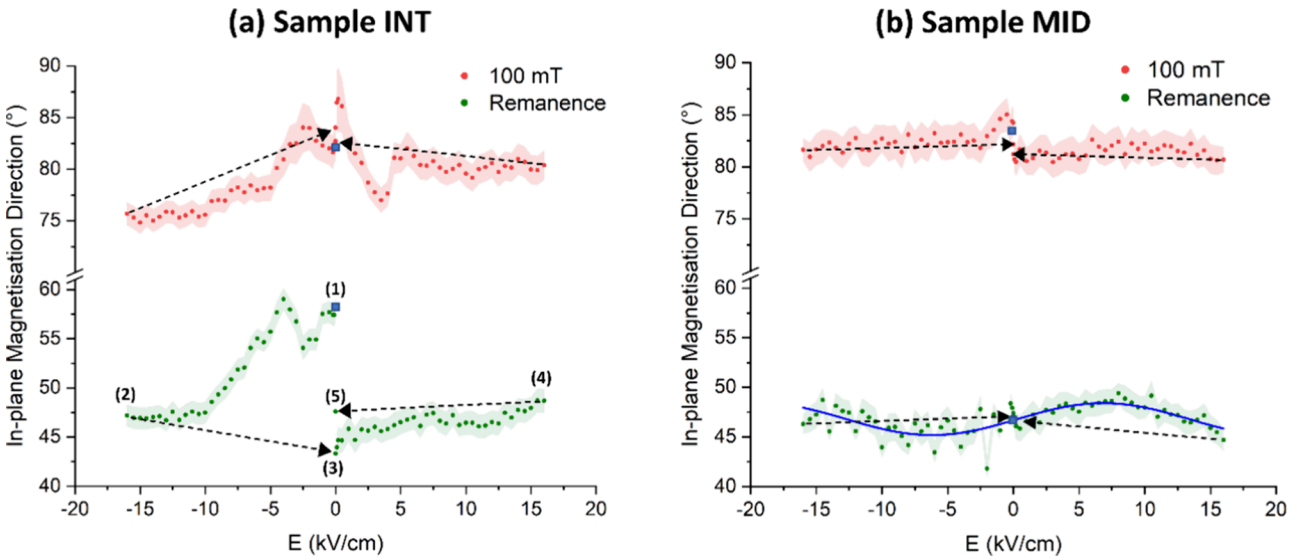

Figure 7. Behavior of the in-plane magnetization direction for (a) Sample INT (Al (3 nm)/^{nat}Fe (4 nm)/^{57}Fe (1 nm)/PMN-PT) and (b) Sample MID (Al (3 nm)/^{nat}Fe (2 nm)/^{57}Fe (1 nm)/^{nat}Fe (2 nm)/PMN-PT) under simultaneous application of *in situ* electric and magnetic fields. The black dashed arrows depict the ramping down of the electric field from −16 and +16 kV/cm to the respective remanent polarization states (0^- and 0^{-+}). The red and green shaded regions depict the error bar on the respective data sets. The blue curve in panel (b) is a guide to the eye. The numbers (1) to (5) depict the electric field history of the samples, and the blue squares represent the electrically pristine state (1). For clarity, the numbers (1) to (5) are depicted only on one curve, but all measurements follow the same sequence.

anisotropy of Fe. A hint of this additional anisotropy component is also seen in the presence of either one- or two-step hysteresis loops depending on the orientation of the applied magnetic field as depicted in Figure 4 a. These two kinds of hysteresis loops imply that the anisotropy of the Fe film is a superposition of intrinsic cubic anisotropy and additional uniaxial anisotropy.[56,57] As a result of the superimposed magnetic anisotropy, the in-plane easy axis of the Fe (5 nm)/PMN-PT system does not lie exactly along the expected 45° direction, but rather, it lies along ∼60 ± 2°. The additional uniaxial anisotropy originates at the Fe/PMN-PT interface, as discussed below.

Probing the Magnetization Direction at and away from the Fe/PMN-PT Interface. To understand the effect of an applied electric field on the magnetization direction of the Fe/PMN-PT system and its depth dependence within the Fe layer, the magnetic responses of Sample INT and Sample MID were analyzed using NFS of synchrotron radiation. Figures 5 and 6 depict the fitted NFS spectra for Sample INT and MID with the ^{57}Fe probe layer at and away from the Fe/PMN-PT interface, respectively, under the influence of the applied electric and magnetic fields. From the NFS fits for both samples, at all applied electric and magnetic field values throughout the experiment, a hyperfine field, B_{hf} ∼ 33 T, corresponding to the bulk B_{hf} value for ferromagnetic metallic Fe (33.3 T[58]) was found. This implies that the Fe/PMN-PT heterostructure, more specifically, the Fe/PMN-PT interface, is electrochemically stable under relatively large values of applied electric fields irrespective of the polarity and no electrically induced magnetic dead layers are formed (as was observed in other material systems).[45,46,59] Since the B_{hf} direction is antiparallel to the net magnetic moment of the ^{57}Fe nuclei,[60] the B_{hf} direction of the ^{57}Fe probe layers derived from the NFS fits provides direct information on the local magnetization direction at and away from the Fe/PMN-PT interface. For the geometry of the NFS measurements depicted in Figure 2, the B_{hf} direction is defined with respect to the synchrotron X-ray beam direction. For example, for a system possessing in-plane magnetization, if the fit (using CONUSS[52]) of the NFS spectrum gives B_{hf} direction = 0° (90°), then the magnetization lies parallel (perpendicular) to the direction of propagation of the synchrotron X-ray beam. For the Fe/PMN-PT samples investigated in this work with the experimental conditions depicted in Figure 2, this further implies that when the B_{hf} direction = 0°, magnetization lies perpendicular to the direction of the applied magnetic field. On the other hand, when the B_{hf} direction = 90°, magnetization lies parallel to and therefore aligned along the direction of the applied magnetic field.

Figure 7 depicts the variation of the in-plane magnetization direction of the probe layer at and away from the Fe/PMN-PT interface under the application of *in situ* electric and/or magnetic fields, as determined from the fits of the NFS time spectra. The order of measurements and, hence, electric field history of the samples are indicated with numbers in Figure 7 a: starting from the electrically pristine state at (1) E = 0 kV/cm, the electric field is increased in the negative direction, and NFS spectra (in 100 mT and at remanence) are recorded at each electric field step up to (2) E = −16 kV/cm. From (2), the electric field is decreased to zero at (3) 0^- and no NFS spectra are recorded in this branch, except at the negative polarization remanent state of 0^-. The electric field is then increased in the positive direction with the NFS spectra being recorded at each electric field step up to (4) E = +16 kV/cm. From (4), the electric field is decreased to zero at (5) 0^{-+} and, again, no NFS spectra are recorded in this branch, except at the final remanent polarization state of 0^{-+}. This order has been followed for both Sample INT and Sample MID. The magnetization direction at the starting electrically pristine state, (1) E = 0 kV/cm state, is marked with a blue square to make it visually more differentiable from the (3) 0^- and (5) 0^{-+} states.

Local Magnetization Direction at E = 0 kV/cm. At (1) E = 0 kV/cm, the azimuthal magnetization direction of the

https://doi.org/10.1021/acsaelm.3c01800
ACS Appl. Electron. Mater. 2024, 6, 2289−2300

interfacial ^{57}Fe probe layer in magnetic remanence (green data set of Figure 7 a) is 58.0 ± 1.1°. This result is consistent with the ∼60 ± 2° direction of the magnetic easy axis for the Fe (5 nm) film as observed in the MOKE measurements (Figure 4 b) at E = 0 kV/cm. In contrast, the magnetization direction of the ^{57}Fe probe layer 2 nm away from the interface in magnetic remanence (green data set of Figure 7 b) is 47.4 ± 0.9°, which is consistent with the direction of the 45° expected bulk easy axis for pure cubic magnetocrystalline anisotropy dominant systems, as mentioned previously. This further implies that magnetic anisotropy for the Fe (5 nm) film (as observed in MOKE) is highly influenced by the Fe/PMN-PT interface.

The origin of the uniaxial anisotropy contribution can be linked to the lattice mismatch between the Fe film and the PMN-PT substrate and/or to the local microscopic irregularities on the PMN-PT surface. The latter is due to the fact that any crystal surface with intrinsic 4-fold symmetry consists of an arrangement of steps even if it appears to be macroscopically flat. These steps can locally break the expected 4-fold symmetry to uniaxial symmetry.[61] It is therefore possible that the interfacial Fe layers are subjected to such local irregularities on the surface of the PMN-PT substrate, causing elongation of the Fe grains, which can further give rise to additional uniaxial anisotropy.

Local Magnetization Direction under Simultaneous Application of Electric and Magnetic Fields. Under the simultaneous application of electric and magnetic fields, a significant difference can be observed in the behavior of the in-plane magnetization direction at and away from the Fe/PMN-PT interface. The behavior of the interfacial ^{57}Fe probe layer (Sample INT) under simultaneous application of *in situ* electric and magnetic fields is depicted in Figure 7 a. It can be seen that in an applied 100 mT magnetic field (red data set of Figure 7 a), the magnetization direction does not fully align with the direction of the applied magnetic field (90°). Initially, at E = 0 kV/cm, the magnetization direction lies at 82.4 ± 1.7°. Upon applying negative electric fields, the magnetization direction rotates to a maximum value of 84.0 ± 2.1° at E = −2.5 kV/cm, which is close to the electric coercive field of the PMN-PT substrate ($|E_C|$ = 2.3 ± 0.2 kV/cm from the S−E response of the PMN-PT substrate depicted in Figure 1 c) where ferroelectric polarization rotates in-plane. Increasing the electric field to E = −10 kV/cm gradually rotates the magnetization direction further away from the direction of the applied magnetic field (90°) to 75.6 ± 1.1°. Further increasing the electric field shows no additional significant changes in the magnetization direction with a final value of 75.7 ± 1.1° recorded at E = −16 kV/cm. After the electric field is ramped down to 0^-, the magnetization direction lies at 84.0 ± 1.1°. Upon switching the polarity and increasing the electric field from 0^- to +16 kV/cm, a peak at E = +0.2 kV/cm is observed where the magnetization direction lies at 86.8 ± 3.1°. This value of electric field is far from the E_C of PMN-PT, and hence, such sharp changes in the magnetization direction are not expected from the electric field-induced strain effects of the substrate. Upon increasing the electric field, the magnetization direction gradually rotates away from the direction of the applied magnetic field (90°) to a maximum value of 77.0 ± 1.2° at E = +3.5 kV/cm. This is close to the E_C of PMN-PT and, although inverted, can still be related to the in-plane ferroelectric polarization rotation, which is sensed by the interfacial ^{57}Fe probe layer. Further increasing the electric field from E = +5 kV/cm leads to negligible variation in the magnetization direction with a final value of 80.4 ± 1.4° at E = +16 kV/cm. After ramping down the electric field to the remanent polarization state 0^{-+}, the magnetization direction lies at 82.7 ± 1.1°. Hence, the magnetization direction of the ^{57}Fe probe layer at the interface under simultaneous application of electric and magnetic fields shows the strongest variation around the E_C of the PMN-PT substrate and is therefore reminiscent of its electric field-induced butterfly-like strain behavior (Figure 1 c).[25,34] For a pure butterfly strain-mediated response, the behavior of the magnetization direction as a function of the applied electric fields should also follow the strain response and, therefore, be volatile at E = 0^- and 0^{-+} (Figure 1 c).[25,62] However, when the magnetic field is turned off and the magnetization direction is no longer influenced by the Zeeman energy of the applied magnetic field, depending on the polarization state of PMN-PT (at E = 0^- and 0^{-+} corresponding to points (3) and (5) in the green data set of Figure 7 a), two clear and distinct magnetization directions are observed. This behavior of the magnetization direction is less significant under the influence of the applied magnetic field (84.0 ± 1.1° and 82.7 ± 1.1° recorded at E = 0^- and 0^{-+}, respectively, in the red data set of Figure 7 a) where it is strongly influenced by the Zeeman energy. Hence, in addition to strain, the Fe/PMN-PT interface is also subjected to remanent polarization-induced charge, which modifies the magnetization direction via the charge screening effect.[22] These results suggest that a coexistence of strain and charge effects stemming from the electric-field effect on the PMN-PT substrate governs the magnetization direction of the ∼1 nm ^{57}Fe interfacial probe layer via magnetoelectroelastic effects.[22−24] For the charge effect to be negligible, the probe layer would have to be placed farther away from the Fe/PMN-PT interface to overcome the Thomas−Fermi screening length for Fe, which is ∼1−2 unit cells or ∼0.3−0.6 nm.[59,63] Therefore, under simultaneous application of *in situ* electric and magnetic fields, the magnetization direction of the Fe/PMN-PT interface is dominated by electric field-induced strain and charge effects originating in the PMN-PT substrate, which overcomes the Zeeman energy of the applied magnetic field.

When the magnetic field is turned off, i.e., in magnetic remanence (note that the electric field is always on in the experiment), the magnetization direction at the interface relaxes away from the applied magnetic field direction (90°) as depicted in the green data set of Figure 7 a. Interestingly, it retains a similar variation to that observed under simultaneous application of electric and magnetic fields (red data set of Figure 7 a) only in the negative electric field regime wherein the sample is subjected to applied electric fields for the first time. Another interesting observation is that for the first few negative electric fields, the magnetization direction rotates from 58.0 ± 1.1° at E = 0 kV/cm to 54.1 ± 1.2° at E = −2.5 kV/cm, which is in the vicinity of the E_C of the PMN-PT substrate. With a further increase in the electric field, the magnetization direction rotates to 47.5 ± 1.1° at E = −10 kV/cm, which is close to the expected magnetic easy axis direction (45°) for the Fe/PMN-PT system. Further increasing the electric field shows no additional significant changes in the magnetization direction with a final value of 47.2 ± 1.1° recorded at E = +16 kV/cm. After the electric field is ramped down to 0^-, the magnetization direction lies at 43.3 ± 1.3°. This is different from the direction observed at E = 0 kV/cm (58.0 ± 1.1°) and is close to the expected magnetic easy axis for the system. Therefore, the application of the large negative

https://doi.org/10.1021/acsaelm.3c01800
ACS Appl. Electron. Mater. 2024, 6, 2289−2300

electric fields ($\sim E \geq -10$ kV/cm) suppresses the post-growth uniaxial contribution to the total magnetic anisotropy. Upon switching the polarity and applying electric fields from 0^- to E = +7.5 kV/cm, the magnetization direction is observed to gradually rotate from 43.3 ± 1.3° to 47.4 ± 1.2°, respectively. Further increasing the electric field shows no significant changes in the magnetization direction with a final value of 48.7 ± 1.2° recorded at E = +16 kV/cm. After the electric field was ramped down to 0^{-+}, the magnetization direction was observed to lie at 47.6 ± 1.2°. Therefore, depending on the polarization state of PMN-PT, i.e., either $E = 0^-$ or 0^{-+}, two clear and distinct magnetization directions are observed (43.3 ± 1.3° and 47.6 ± 1.2°, respectively). Additionally, it must be noted that (i) the decrease in the magnetization direction upon application of the first (in this case, negative) electric fields and (ii) a significant difference in the magnetoelectric response of the magnetization direction in negative and positive electric fields were only observed when the interfacial probe layer was analyzed in magnetic remanence after application of 100 mT magnetic field. Interestingly, this behavior can be attributed to the turning "on" and "off" of the applied magnetic field in the experiment. For similar (001)-oriented PMN-28PT single-crystal substrates, it was shown (Figure 4a in ref 64) that the interplanar spacing (d) and, hence, strain response derived from it in the electric remanent state of every applied electric field underwent an initial decrease up to a critical electric field value that was close to E_C. This was attributed to FE domain motion in the PMN-28PT substrate arising due to reorientation of the initial polarization such that a more stable configuration is attained with respect to the direction of the first applied electric fields.[64] After such reorientation, the electric field-induced strain did not undergo significant changes, even when critical points of change ($\pm E_C$) were encountered. Our results of the interfacial ^{57}Fe probe layer's magnetization direction show similar behavior when measured in magnetic remanence after application of 100 mT magnetic field, i.e., when the magnetic field was turned "on" and "off" (green data set of Figure 7 a). Moreover, it is known that the in-plane lattice parameter in regions that are close to the surface (outside) is larger than in the bulk (inside) region in PMN-30PT substrates, which is due to relaxation of internal stresses in the latter region.[65] Now, under the influence of simultaneously applied electric and magnetic fields, the Fe film is subjected to in-plane magnetostrictive strain directly from the applied magnetic field and indirectly via the strain-mediated converse magnetoelectric effects due to the applied electric field. Turning "off" the magnetic field relaxes the former, which further has the potential to modify the interplanar spacing, hence, the lattice parameter and, ultimately, the strain in the near-surface region of the PMN-PT substrate, which is in contact with the Fe film. Therefore, turning "on" and "off" the magnetic field in this work can be seen to have a similar effect on the electric field-induced strain in the near-surface region of the PMN-PT substrate, which is in turn sensed by the interfacial ^{57}Fe probe layer.

The in-plane magnetization orientation of the ^{57}Fe probe layer away from the Fe/PMN-PT interface in the 100 mT applied magnetic field as a function of the electric field is depicted in the red data set of Figure 7 b. It can be seen that magnetization does not align completely with the applied magnetic field, but it is closer to the 90° orientation as compared to the ^{57}Fe probe layer at the Fe/PMN-PT interface (red data set of Figure 7 a). Throughout the application of both polarities of the electric field, it can be seen that the magnetization direction of the ^{57}Fe probe layer away from the Fe/PMN-PT interface shows no significant variation and has a peak value of 85.0 ± 1.6° at E = −0.5 kV/cm. This value of the electric field is far smaller than the E_C of PMN-PT and hence cannot be related to effects due to in-plane ferroelectric polarization. For the remainder of the negative and positive electric fields, the magnetization direction can be averaged to lie at ∼82°. Therefore, 2 nm away from the Fe/PMN-PT interface, under simultaneous application of electric and magnetic fields, the Zeeman energy due to the latter dominates the behavior of the magnetization direction.

In magnetic remanence, the magnetization direction relaxes to ∼45° (Figure 7 b), which is consistent with the expected easy axis for the Fe/PMN-PT system. Moreover, it shows a minor variation with the applied electric field that is antisymmetric about E = 0 kV/cm (the blue line is a guide to the eye). Up to ±5 kV/cm, the behavior of the magnetization direction varies almost proportional to the applied electric field. After that, in negative (positive) electric fields, the magnetization direction gradually increases (decreases). The reason behind such clear and distinct differences in the magnetization direction behavior at (Figure 7 a) and away (Figure 7 b) from the Fe/PMN-PT interface is not straightforward. Moreover, the small variation of the magnetization direction in the region away from the interface is striking but, at the same time, not completely unexpected. It was recently shown that the magnetic response observed via magnetometry measurements can be quite different from the magnetic response on the surface of the FM film in FM/PMN-PT systems due to additional contributions of in-plane shear strains and electric field-induced cracks of the substrate.[35,40] During the polarization switching process of a Ni/(011)-$PMN_{0.68}$-$PT_{0.32}$ system, it was shown[40] that an in-plane shear strain (∼0.14%) competed significantly with the normal macroscopic strain (∼0.2%) associated with non-180° ferroelectric domain switching, which causes the in-plane magnetization direction on the surface of the Ni film to deviate from the expected 90° rotation and rotate by ± 62°, a sub-90° rotation. Additionally, non-90° rotation of magnetic domain directions with a wide distribution of angles was observed on the surface of an Fe/(001)-$PMN_{0.6}$-$PT_{0.4}$ system,[35] which was mainly linked to changes in the morphology of the Fe surface due to electric field-induced crack formations originating in the substrate. Moreover, the largest distribution of magnetization rotation with angles ≤ 10° was observed upon polarization switching for a particular position on the Fe surface (50 μm field of view), which was devoid of any electric field-induced cracks.[35] These reports suggest that the effect of an electric field on the magnetization direction is quite complex on the surface of the FM film in contact with such PMN-PT substrates, i.e., in the region away from the FM/PMN-PT interface. The behavior of the magnetization direction 2 nm away from the Fe/PMN-PT interface reported in this work provides added evidence of the unexpected yet consistent[35] minor (≤ 10°) variation as a function of the applied electric fields irrespective of polarization switching (green data set of Figure 7 b). Hence, our results show that the magnetoelectric response of the magnetization direction in FM/PMN-PT heterostructures depicts a variation within the depth of the FM and the global/volume-averaged magnetic/magnetoelectric response of these systems is highly influenced by the FM/PMN-PT interface.

https://doi.org/10.1021/acsaelm.3c01800
ACS Appl. Electron. Mater. 2024, 6, 2289−2300

CONCLUSIONS

In summary, the global and local magnetic properties of Fe/PMN-PT heterostructures were studied using magneto-optic Kerr effect (MOKE) magnetometry and nuclear forward scattering (NFS) of synchrotron radiation, respectively. In the electrically pristine state, the MOKE results show that the in-plane magnetic anisotropy of the Fe (5 nm)/PMN-PT system is composed of dominant 4-fold magnetocrystalline anisotropy superimposed by a uniaxial magnetic anisotropy component. The NFS results reveal that uniaxial anisotropy stems from the Fe/PMN-PT interface. The global anisotropy of the Fe (5 nm)/PMN-PT system observed in MOKE is, therefore, highly influenced by the Fe/PMN-PT interface.

Further, although Sample INT and Sample MID are structurally and magnetically identical, the NFS results show that the magnetization direction behaves differently at vs away from the Fe/PMN-PT interface. At the Fe/PMN-PT interface, the magnetization direction is strongly influenced by strain- and charge-mediated effects originating from PMN-PT. However, only 2 nm away from the Fe/PMN-PT interface, the magnetization direction shows a minor variation with the applied electric field, which is consistent with previous reports. Therefore, the magnetoelectric response of the magnetization direction shows depth-specific behavior even for this ultrathin 5 nm Fe layer.

These results take the current understanding of the electric-field control of magnetism in such FM/PMN-PT heterostructures a major step further by establishing that alongside previously reported lateral variations of the magnetization direction on the surface of the FM, it also displays a variation through the thickness of the film. Therefore, these results provide further insight and atomic-level information toward a deeper understanding of the electric-field control of magnetism in FM/FE heterostructures.

AUTHOR INFORMATION

Corresponding Author

Michelle Rodrigues − *Quantum Solid-State Physics (QSP), KU Leuven, Leuven 3001, Belgium;* orcid.org/0000-0003-4935-2659; Email: michelle.rodrigues@kuleuven.be

Authors

Sergey Basov − *Quantum Solid-State Physics (QSP), KU Leuven, Leuven 3001, Belgium*

Ivan Madarevic − *imec, Leuven 3001, Belgium; Quantum Solid-State Physics (QSP), KU Leuven, Leuven 3001, Belgium*

Thomas Saerbeck − *Institut Laue-Langevin, Grenoble Cedex 9 38042, France*

Matteo Ferroni − *Department of Civil, Environmental, Architectural Engineering and Mathematics (DICATAM), Università di Brescia, Brescia 43-25123, Italy; National Research Council−Institute for Microelectronics and Microsystems (CNR-IMM), Bologna 101-40129, Italy*

Patrick Breckner − *Department of Materials and Earth Sciences, Technical University of Darmstadt, Darmstadt 64287, Germany*

Daniel Isaia − *Department of Materials and Earth Sciences, Technical University of Darmstadt, Darmstadt 64287, Germany*

Lovro Fulanović − *Department of Materials and Earth Sciences, Technical University of Darmstadt, Darmstadt 64287, Germany*

Atefeh Jafari − *Deutsches Elektronen Synchrotron DESY, Hamburg 22607, Germany;* orcid.org/0000-0001-6011-1720

Ilya Sergueev − *Deutsches Elektronen Synchrotron DESY, Hamburg 22607, Germany*

Olaf Leupold − *Deutsches Elektronen Synchrotron DESY, Hamburg 22607, Germany*

Margriet J. Van Bael − *Quantum Solid-State Physics (QSP), KU Leuven, Leuven 3001, Belgium;* orcid.org/0000-0002-7687-4498

André Vantomme − *Quantum Solid-State Physics (QSP), KU Leuven, Leuven 3001, Belgium;* orcid.org/0000-0001-9158-6534

Kristiaan Temst − *Quantum Solid-State Physics (QSP), KU Leuven, Leuven 3001, Belgium; imec, Leuven 3001, Belgium*

Complete contact information is available at: https://pubs.acs.org/10.1021/acsaelm.3c01800

Author Contributions

The manuscript was written through contributions of all authors. All authors have given approval to the final version of the manuscript.

Notes

The authors declare no competing financial interest.

ACKNOWLEDGMENTS

The work was funded by KU Leuven, C1 grant number C14/18/074, the Fund for Scientific Research-Flanders (FWO), and the FWO-FNRS WEAVE program. The TEM measurements were performed at CNR-IMM, Bologna, Italy, under the framework of the Nanoscience Foundry and Fine Analysis (NFFA Europe-Pilot grant nr. 101007417−project proposal ID 479). The *S*−*E* measurements of the PMN-PT substrates were conducted at The Department of Materials and Earth Sciences, Technical University of Darmstadt, Darmstadt, Germany. The authors would like to thank Dr. Wolfgang Sturhahn and Prof. Dr. Stefaan Cottenier for fruitful discussions and Ing. Bas Opperdoes for technical support. The authors would also like to thank the research staff and technicians at the D17 reflectometer at ILL, Grenoble, France, and at the P01 beamline, Petra III at DESY, Hamburg, Germany, for provision of the experimental facilities to conduct the nuclear forward scattering measurements.

REFERENCES

(1) Ohno, H.; Chiba, D.; Matsukura, F.; Omiya, T.; Abe, E.; Dietl, T.; Ohno, Y.; Ohtani, K. Electric-Field Control of Ferromagnetism. *Nature* **2000**, *408* (6815), 944−946.

(2) Hu, J. M.; Li, Z.; Chen, L. Q.; Nan, C. W. High-Density Magnetoresistive Random Access Memory Operating at Ultralow Voltage at Room Temperature. *Nat. Commun.* **2011**, *2* (1), 553.

(3) Song, C.; Cui, B.; Li, F.; Zhou, X.; Pan, F. Recent Progress in Voltage Control of Magnetism: Materials, Mechanisms, and Performance. *Prog. Mater. Sci.* **2017**, *87*, 33−82.

(4) Ramesh, R.; Manipatruni, S. Electric Field Control of Magnetism. *Proc. R. Soc. A* **2021**, *477* (2251), 20200942 DOI: 10.1098/rspa.2020.0942.

(5) Fiebig, M. Revival of the Magnetoelectric Effect. *J. Phys. D. Appl. Phys.* **2005**, *38* (8), R123−R152.

(6) Ma, J.; Hu, J.; Li, Z.; Nan, C. W. Recent Progress in Multiferroic Magnetoelectric Composites: From Bulk to Thin Films. *Adv. Mater.* **2011**, *23* (9), 1062−1087.

(7) Fusil, S.; Garcia, V.; Barthélémy, A.; Bibes, M. Magnetoelectric Devices for Spintronics. *Annu. Rev. Mater. Res.* **2014**, *44*, 91−116.

(8) Spaldin, N.; Multiferroics, A. Past, Present, and Future. *MRS Bull.* **2017**, *42* (5), 385−389.
(9) Manipatruni, S.; Nikonov, D. E.; Lin, C. C.; Gosavi, T. A.; Liu, H.; Prasad, B.; Huang, Y. L.; Bonturim, E.; Ramesh, R.; Young, I. A. Scalable Energy-Efficient Magnetoelectric Spin−Orbit Logic. *Nature* **2019**, *565* (7737), 35−42.
(10) Hill, N. A. Why Are There so Few Magnetic Ferroelectrics? *J. Phys. Chem. B* **2000**, *104* (29), 6694−6709.
(11) Scott, J. F. Room-temperature multiferroic magnetoelectrics. *NPG Asia Mater.* **2013**, *5* (10), e72.
(12) Gajek, M.; Bibes, M.; Fusil, S.; Bouzehouane, K.; Fontcuberta, J.; Barthélémy, A.; Fert, A. Tunnel Junctions with Multiferroic Barriers. *Nat. Mater.* **2007**, *6* (4), 296−302.
(13) Bibes, M.; Barthélémy, A. Towards a Magnetoelectric Memory. *Nat. Mater.* **2008**, *7* (6), 425−426.
(14) Manipatruni, S.; Nikonov, D. E.; Young, I. A. Beyond CMOS Computing with Spin and Polarization. *Nat. Phys.* **2018**, *14* (4), 338−343.
(15) Gupta, R.; Kotnala, R. K. A Review on Current Status and Mechanisms of Room-Temperature Magnetoelectric Coupling in Multiferroics for Device Applications. *J. Mater. Sci.* **2022**, *57* (27), 12710−12737.
(16) Garcia, V.; Bibes, M.; Barthélémy, A. Artificial Multiferroic Heterostructures for an Electric Control of Magnetic Properties. *Comptes Rendus Phys.* **2015**, *16* (2), 168−181.
(17) Hu, J. M.; Chen, L. Q.; Nan, C. W. Multiferroic Heterostructures Integrating Ferroelectric and Magnetic Materials. *Adv. Mater.* **2016**, *28* (1), 15−39.
(18) Fernandes Vaz, C. A.; Staub, U. Artificial Multiferroic Heterostructures. *J. Mater. Chem. C* **2013**, *1* (41), 6731−6742.
(19) Scott, J. F. Multiferroic Memories. *Nat. Mater.* **2007**, *6* (4), 256−257.
(20) Leung, C. M.; Li, J.; Viehland, D.; Zhuang, X. A Review on Applications of Magnetoelectric Composites: From Heterostructural Uncooled Magnetic Sensors, Energy Harvesters to Highly Efficient Power Converters. *J. Phys. D. Appl. Phys.* **2018**, *51* (26), 263002.
(21) Pradhan, D. K.; Kumari, S.; Rack, P. D. Magnetoelectric Composites: Applications, Coupling Mechanisms, and Future Directions. *Nanomaterials* **2020**, 18−20.
(22) Nan, T.; Zhou, Z.; Liu, M.; Yang, X.; Gao, Y.; Assaf, B. A.; Lin, H.; Velu, S.; Wang, X.; Luo, H.; Chen, J.; Akhtar, S.; Hu, E.; Rajiv, R.; Krishnan, K.; Sreedhar, S.; Heiman, D.; Howe, B. M.; Brown, G. J.; Sun, N. X. Quantification of Strain and Charge Co-Mediated Magnetoelectric Coupling on Ultra-Thin Permalloy/PMN-PT Interface. *Sci. Rep.* **2014**, *4* (1), 1−6.
(23) Heidler, J.; Fechner, M.; Chopdekar, R. V.; Piamonteze, C.; Dreiser, J.; Jenkins, C. A.; Arenholz, E.; Rusponi, S.; Brune, H.; Spaldin, N. A.; Nolting, F. Magnetoelectroelastic Control of Magnetism in an Artificial Multiferroic. *Phys. Rev. B* **2016**, *94* (1), 1−7.
(24) Rondinelli, J. M.; Stengel, M.; Spaldin, N. A. Carrier-Mediated Magnetoelectricity in Complex Oxide Heterostructures. *Nat. Nanotechnol.* **2008**, *3* (1), 46−50.
(25) Thiele, C.; Dörr, K.; Bilani, O.; Rödel, J.; Schultz, L. Influence of Strain on the Magnetization and Magnetoelectric Effect in La0.7 A0.3 Mn O3 PMN-PT (001) (A = Sr, Ca). *Phys. Rev. B - Condens. Matter Mater. Phys.* **2007**, *75* (5), No. 054408.
(26) Noheda, B.; Cox, D. E.; Shirane, G.; Gao, J.; Ye, Z. G. Phase Diagram of the Ferroelectric Relaxor (1-x) PbMg1/3Nb2/3O3-XPbTiO3. *Phys. Rev. B - Condens. Matter Mater. Phys.* **2002**, *66* (5), 541041−5410410.
(27) Rajan, K. K.; Shanthi, M.; Chang, W. S.; Jin, J.; Lim, L. C. Dielectric and Piezoelectric Properties of [0 0 1] and [0 1 1]-Poled Relaxor Ferroelectric PZN-PT and PMN-PT Single Crystals. *Sensors Actuators, A Phys.* **2007**, *133* (1), 110−116.
(28) Zhang, S.; Zhao, Y. G.; Li, P. S.; Yang, J. J.; Rizwan, S.; Zhang, J. X.; Seidel, J.; Qu, T. L.; Yang, Y. J.; Luo, Z. L.; He, Q.; Zou, T.; Chen, Q. P.; Wang, J. W.; Yang, L. F.; Sun, Y.; Wu, Y. Z.; Xiao, X.; Jin, X. F.; Huang, J.; Gao, C.; Han, X. F.; Ramesh, R. Electric-Field Control of Nonvolatile Magnetization in Co 40Fe 40B 20/Pb(Mg 1/3Nb 2/3) 0.7Ti 0.3O 3 Structure at Room Temperature. *Phys. Rev. Lett.* **2012**, *108* (13), No. 137203.
(29) Avula, S. R. V.; Heidler, J.; Dreiser, J.; Vijayakumar, J.; Howald, L.; Nolting, F.; Piamonteze, C. Study of Magneto-Electric Coupling between Ultra-Thin Fe Films and PMN-PT Using X-Ray Magnetic Circular Dichroism. *J. Appl. Phys.* **2018**, *123* (6), 1−6.
(30) Xu, H.; Wang, B.; Qi, J.; Liu, M.; Teng, F.; Hu, L.; Zhang, Y.; Qu, C.; Feng, M. Modulation of Spin Dynamics in Ni/Pb(Mg1/3Nb2/3)O3-PbTiO3Multiferroic Heterostructure. *J. Adv. Ceram.* **2022**, *11* (3), 515−521.
(31) Xu, H.; Huang, K.; Li, C.; Qi, J.; Li, J.; Sun, G.; Wang, F.; Li, H.; Sun, Y.; Ye, C.; Yang, L.; Pan, Y.; Feng, M.; Lü, W. Enhanced Magnetoresistance and Electroresistance at High Temperature in a Nano-Matrix Manganite. *Acta Mater.* **2022**, *238*, No. 118219.
(32) Zhang, Y.; Wang, Z.; Wang, Y.; Luo, C.; Li, J.; Viehland, D. Electric-field induced strain modulation of magnetization in Fe-Ga/Pb(Mg1/3Nb2/3)-PbTiO3 magnetoelectric heterostructures. *J. Appl. Phys.* **2014**, *115* (8), No. 084101, DOI: 10.1063/1.4866495.
(33) Li, P.; Zhao, Y.; Zhang, S.; Chen, A.; Li, D.; Ma, J.; Liu, Y.; Pierce, D. T.; Unguris, J.; Piao, H. G.; Zhang, H.; Zhu, M.; Zhang, X.; Han, X.; Pan, M.; Nan, C. W. Spatially Resolved Ferroelectric Domain-Switching-Controlled Magnetism in Co40Fe40B20/Pb-(Mg1/3Nb2/3)0.7Ti0.3O3Multiferroic Heterostructure. *ACS Appl. Mater. Interfaces* **2017**, *9* (3), 2642−2649.
(34) Zhang, S.; Chen, Q.; Liu, Y.; Chen, A.; Yang, L.; Li, P.; Ming, Z. S.; Yu, Y.; Sun, W.; Zhang, X.; Zhao, Y.; Sun, Y.; Zhao, Y. Strain-Mediated Coexistence of Volatile and Nonvolatile Converse Magnetoelectric Effects in Fe/Pb(Mg1/3Nb2/3)0.7Ti0.3O3 Heterostructure. *ACS Appl. Mater. Interfaces* **2017**, *9* (24), 20637−20647.
(35) Motti, F.; Vinai, G.; Bonanni, V.; Polewczyk, V.; Mantegazza, P.; Forrest, T.; Maccherozzi, F.; Benedetti, S.; Rinaldi, C.; Cantoni, M.; Cassese, D.; Prato, S.; Dhesi, S. S.; Rossi, G.; Panaccione, G.; Torelli, P. Interplay between Morphology and Magnetoelectric Coupling in Fe/PMN-PT Multiferroic Heterostructures Studied by Microscopy Techniques. *Phys. Rev. Mater.* **2020**, *4* (11), No. 114418.
(36) Begué, A.; Ciria, M. Strain-Mediated Giant Magnetoelectric Coupling in a Crystalline Multiferroic Heterostructure. *ACS Appl. Mater. Interfaces* **2021**, *13* (5), 6778−6784.
(37) Zheng, M.; Usami, T.; Taniyama, T. Shear-strain-mediated large nonvolatile tuning of ferromagnetic resonance by an electric field in multiferroic heterostructures. *NPG Asia Mater.* **2021**, *13* (1), 7 DOI: 10.1038/s41427-020-00279-4.
(38) Liu, Y.; Zhao, Y.; Li, P.; Zhang, S.; Li, D.; Wu, H.; Chen, A.; Xu, Y.; Han, X. F.; Li, S.; Lin, D.; Luo, H. Electric-Field Control of Magnetism in Co40Fe40B20/(1-x)Pb(Mg1/3Nb2/3)O3-XPbTiO3-Multiferroic Heterostructures with Different Ferroelectric Phases. *ACS Appl. Mater. Interfaces* **2016**, *8* (6), 3784−3791.
(39) Zhou, C.; Shen, L.; Liu, M.; Gao, C.; Jia, C.; Jiang, C.; Xue, D. Long-Range Nonvolatile Electric Field Effect in Epitaxial Fe/Pb(Mg 1/3 Nb 2/3) 0.7 Ti 0.3 O 3 Heterostructures. *Adv. Funct. Mater.* **2018**, *28* (20), 1707027.
(40) Ghidini, M.; Mansell, R.; Maccherozzi, F.; Moya, X.; Phillips, L. C.; Yan, W.; Pesquera, D.; Barnes, C. H. W.; Cowburn, R. P.; Hu, J.-M.; Dhesi, S. S.; Mathur, N. D. Shear-Strain-Mediated Magnetoelectric Effects Revealed by Imaging. *Nat. Mater.* **2019**, *18* (8), 840−845.
(41) Liu, Z. Q.; Liu, J. H.; Biegalski, M. D.; Hu, J.-M.; Shang, S. L.; Ji, Y.; Wang, J. M.; Hsu, S. L.; Wong, A. T.; Cordill, M. J.; Gludovatz, B.; Marker, C.; Yan, H.; Feng, Z. X.; You, L.; Lin, M. W.; Ward, T. Z.; Liu, Z. K.; Jiang, C. B.; Chen, L. Q.; Ritchie, R. O.; Christen, H. M.; Ramesh, R. Electrically Reversible Cracks in an Intermetallic Film Controlled by an Electric Field. *Nat. Commun.* **2018**, *9* (1), 41.
(42) Röhlsberger, R.; Bansmann, J.; Senz, V.; Jonas, K. L.; Bettac, A.; Meiwes-Broer, K. H.; Leupold, O. Nanoscale Magnetism Probed by Nuclear Resonant Scattering of Synchrotron Radiation. *Phys. Rev. B* **2003**, *67* (24), No. 245412.

(43) Schlage, K.; Röhlsberger, R. Nuclear Resonant Scattering of Synchrotron Radiation: Applications in Magnetism of Layered Structures. *J. Electron Spectrosc. Relat. Phenom.* **2013**, *189*, 187−195.
(44) Röhlsberger, R. *Nuclear Condensed Matter Physics with Synchrotron Radiation*; Springer Tracts in Modern Physics;: Berlin, Heidelberg, 2005; Vol. *208*. doi: DOI: 10.1007/b86125.
(45) Couet, S.; Bisht, M.; Trekels, M.; Menghini, M.; Petermann, C.; Van Bael, M. J.; Locquet, J.; Rüffer, R.; Vantomme, A.; Temst, K. Electric Field-Induced Oxidation of Ferromagnetic/Ferroelectric Interfaces. *Adv. Funct. Mater.* **2014**, *24* (1), 71−76.
(46) Bisht, M.; Couet, S.; Lazenka, V.; Modarresi, H.; Rüffer, R.; Locquet, J.; Van Bael, M. J.; Vantomme, A.; Temst, K. Electric Polarity-Dependent Modification of the Fe/BaTiO 3 Interface. *Adv. Mater. Interfaces* **2016**, *3* (4), 1−6.
(47) Laenens, B.; Planckaert, N.; Demeter, J.; Trekels, M.; L'Abbé, C.; Strohm, C.; Rüffer, R.; Temst, K.; Vantomme, A.; Meersschaut, J. Spin Structure in Perpendicularly Magnetized Fe-FePt Bilayers. *Phys. Rev. B - Condens. Matter Mater. Phys.* **2010**, *82* (10), 1−7.
(48) Lazenka, V.; Lorenz, M.; Modarresi, H.; Bisht, M.; Rüffer, R.; Bonholzer, M.; Grundmann, M.; Van Bael, M. J.; Vantomme, A.; Temst, K. Magnetic spin structure and magnetoelectric coupling in BiFeO3-BaTiO3 multilayer. *Appl. Phys. Lett.* **2015**, *106* (8), No. 082904, DOI: 10.1063/1.4913444.
(49) Wille, H.-C.; Franz, H.; Röhlsberger, R.; Caliebe, W. A.; Dill, F.-U. Nuclear resonant scattering at PETRA III: Brillant opportunities for nano − and extreme condition science. *J. Phys. Conf. Ser.* **2010**, *217*, No. 012008.
(50) Wertheim, G. K. *Mössbauer Effect: Principles and Applications*; New York: Academic Press Inc., 1964. doi: DOI: 10.1016/C2013-0-12103-4.
(51) Principi, G. The Mössbauer Effect: A Romantic Scientific Page. *Metals* **2020**, *10* (8), 992.
(52) Sturhahn, W. CONUSS and PHOENIX: Evaluation of Nuclear Resonant Scattering Data. *Hyperfine Interact.* **2000**, *125* (1−4), 149−172.
(53) Sturhahn, W.; Gerdau, E. Evaluation of Time-Differential Measurements of Nuclear-Resonance Scattering of x Rays. *Phys. Rev. B* **1994**, *49* (14), 9285−9294.
(54) Osgood, R. M.; White, R. L.; Clemens, B. M. Second Order Magneto-Optic Effects in Epitaxial FE(110)/MO(110) Bilayers. *MRS Proc.* **1995**, *384*, 491.
(55) Postava, K.; Jaffres, H.; Schuhl, A.; Nguyen Van Dau, F.; Goiran, M.; Fert, A. R. Linear and quadratic magneto-optical measurements of the spin reorientation in epitaxial Fe films on MgO. *J. Magn. Magn. Mater.* **1997**, *172* (3), 199−208.
(56) Cowburn, R. P.; Gray, S. J.; Ferré, J.; Bland, J. A. C.; Miltat, J. Magnetic Switching and In-Plane Uniaxial Anisotropy in Ultrathin Ag/Fe/Ag(100) Epitaxial Films. *J. Appl. Phys.* **1995**, *78* (12), 7210−7219.
(57) Zhan, Q. f.; Vandezande, S.; Van Haesendonck, C.; Temst, K. Manipulation of in-plane uniaxial anisotropy in Fe/MgO(001) films by ion sputtering. *Appl. Phys. Lett.* **2007**, *91* (12), 122510 DOI: 10.1063/1.2789396.
(58) Hanna, S. S.; Heberle, J.; Littlejohn, C.; Perlow, G. J.; Preston, R. S.; Vincent, D. H. Polarized Spectra and Hyperfine Structure in Fe57. *Phys. Rev. Lett.* **1960**, *4* (4), 177−180.
(59) Radaelli, G.; Petti, D.; Plekhanov, E.; Fina, I.; Torelli, P.; Salles, B. R.; Cantoni, M.; Rinaldi, C.; Gutiérrez, D.; Panaccione, G.; Varela, M.; Picozzi, S.; Fontcuberta, J.; Bertacco, R. Electric Control of Magnetism at the Fe/BaTiO3interface. *Nat. Commun.* **2014**, *5*, 1−9.
(60) Hanna, S. S.; Heberle, J.; Perlow, G. J.; Preston, R. S.; Vincent, D. H. Direction of the Effective Magnetic Field at the Nucleus in Ferromagnetic Iron. *Phys. Rev. Lett.* **1960**, *4* (10), 513−515.
(61) Weber, W.; Back, C. H.; Bischof, A.; Würsch, C.; Allenspach, R. Morphology-Induced Oscillations of the Magnetic Anisotropy in Ultrathin Co Films. *Phys. Rev. Lett.* **1996**, *76* (11), 1940−1943.
(62) Park, S. E.; Shrout, T. R. Ultrahigh Strain and Piezoelectric Behavior in Relaxor Based Ferroelectric Single Crystals. *J. Appl. Phys.* **1997**, *82* (4), 1804−1811.
(63) Maruyama, T.; Shiota, Y.; Nozaki, T.; Ohta, K.; Toda, N.; Mizuguchi, M.; Tulapurkar, A. A.; Shinjo, T.; Shiraishi, M.; Mizukami, S.; Ando, Y.; Suzuki, Y. Large Voltage-Induced Magnetic Anisotropy Change in a Few Atomic Layers of Iron. *Nat. Nanotechnol.* **2009**, *4* (3), 158−161.
(64) Levin, A. A.; Thiele, C.; Paufler, P.; Meyer, D. C. In-Situ X-Ray Investigation of a PbMg1/3Nb2/3O 3−28%PbTiO3 Single-Crystal Plate in an External Electric Field. *Appl. Phys. A Mater. Sci. Process.* **2006**, *84* (1−2), 37−45.
(65) Bai, F.; Wang, N.; Li, J.; Viehland, D.; Gehring, P. M.; Xu, G.; Shirane, G. X-Ray and Neutron Diffraction Investigations of the Structural Phase Transformation Sequence under Electric Field in 0.7Pb(Mg 1/3Nb 2/3)-0.3PbTiO 3 Crystal. *J. Appl. Phys.* **2004**, *96* (3), 1620−1627.

https://doi.org/10.1021/acsaelm.3c01800
ACS Appl. Electron. Mater. 2024, 6, 2289−2300